Monolayer $MoSe_2$ based Tunneling Field Effect Transistor for Ultra-Sensitive Strain Sensing

Prabhat K. Dubey, *Student Member*, *IEEE*, Nivasan Yogeswaran, Fengyuan Liu, Anastasios Vilouras, Brajesh K. Kaushik, *Senior Member, IEEE*, Ravinder Dahiya, *Fellow IEEE*

***Abstract*—This paper presents a detailed investigation of the impact of mechanical strain on transition metal dichalcogenide (TMD) material based tunneling field-effect transistor (TFET). First, the impact of mechanical strain on material parameters of $MoSe_2$ is calculated using the first principle of density functional theory (DFT) under meta generalized gradient approximation (MGGA). The device performance of the TMD TFET has been studied by solving the self-consistent 3D Poisson and Schrodinger equations in non-equilibrium Green's function (NEGF) framework. The results demonstrate that both I_{ON} and I_{OFF} increase with uniaxial tensile strain, however, the change in I_{ON}/I_{OFF} ratio remains small. This strain dependent performance change in TMD TFET has been utilized to design an ultra-sensitive strain sensor. The device shows a sensitivity ($\Delta I_{DS}/I_{DS}$) of 3.61 for a strain of 2%. Due to the high sensitivity to the strain, these result shows the potential of using $MoSe_2$ TFET as a flexible strain sensor. Furthermore, the strained TFET is analyzed for backend circuit performance. It is observed that the speed and energy efficiency of 10 stage inverter chain based on controlled strain improve substantially in comparison to unstrained TFET.**

***Index Terms*—TMD TFET, transition metal dichalcogenides, uniaxial strain.**

I. Introduction

THE flexible and stretchable electronics has attracted increasing attention due to the promise it holds for advances in various applications including health monitoring, robotics and e-skin [1]-[5] . Some of these applications demand high-performance and in this regard the modest performance of organic semiconductors based devices may be insufficient. The widely used inorganic semiconductors such as silicon (Si) based devices offer excellent performance, but owing to their brittle nature they do not offer much in terms of mechanical flexibility. Through innovative methods such as wafer or chip thinning [6] and ultra-thin electronic layers by printing Si nanowires [7],[8], there has been few attempts to overcome the above issues. However, the handling of delicate ultra-thin chips and large scale uniform printing of Si based electronic layers are still challenging tasks [9]. Meanwhile, 2D materials have emerged as potential alternatives as they offer excellent properties such as atomically thin layered structure, absence of surface dangling bonds, superior electronic property and natural compatibility with flexible electronics [10]–[14]. Specifically, mono- and few layer of $MoSe_2$ have been regarded as a promising candidate for flexible electronics due to their excellent semiconducting behavior, a tunable band gap, better mechanical stability [15], [16]. Further, the piezoresistive effect in $MoSe_2$ [17], specially the reduction in band gap with an increase in uniaxial stretching strain, can offer new functionalities such as strain, pressure, and acceleration sensing. In fact, various transition metal dichalcogenide (TMD) materials such as MoS_2, $MoSe_2$ and $MoTe_2$ show strain dependent properties. This is attractive as instead of attempting to compensate the mechanically bending induced variation, they could be exploited to develop the devices for sensing applications [18], [19]. Among these, MoS_2 is not suitable for tunnel FET applications due to its large band gap of 1.8 eV, which significantly reduces the band-to-band tunneling probability. Semiconducting $MoTe_2$ (2H-phase) suffers from the stability issue [15], [20]. Therefore, this is not feasible for reliable FET realization, especially under external strain. $MoSe_2$, on the other hand, has a comparatively lower band gap (1.39 eV) than MoS_2, which is more suitable for TFET application. Also, it shows a better stability in 2H-phase and thus makes a good channel material for the designing steep slope strain sensitive TFET.

Herein we present the impact of the strain on $MoSe_2$ based tunneling field-effect transistors (TFET) and its potential use for strain sensing. Compared to the conventional MOSFETs, the TFETs exhibit much steeper slope in the transfer characteristics with subthreshold swing lower than the 60 mV/decade [21]–[24]. This special property makes TFETs attractive in terms of power efficiency and hence as important building blocks for next generation of high-performance flexible and stretchable electronics. The steep slope in TFETs is attributed to the band-to-band tunneling transport mechanism instead of thermal generation-based transport. The tunneling probability (T) of the charge carriers in TFETs is exponentially dependent on the band gap (E_g) of the material as [21]:

This work is supported in part by the British Council and Science and Engineering Research Board (SERB) through Newton-Bhabha Mobility scheme and by Engineering and Physical Sciences Research Council (EPSRC) through Engineering Fellowship for Growth (EP/R029644/1) and Heteroprint Programme Grant (EP/R03480X/1).

Prabhat Kumar Dubey and Brajesh Kumar Kaushik are with the Microelectronics and VLSI Group, Department of Electronics and Communication Engineering, IIT Roorkee, Roorkee, India.
Nivasan Yogeshwaran, Fengyuan Liu, Anastasios Vilouras and Ravinder Dahiya are with the BEST Group, University of Glasgow, Glasgow, UK.
Correspondence to – Ravinder.Dahiya@glasgow.ac.uk

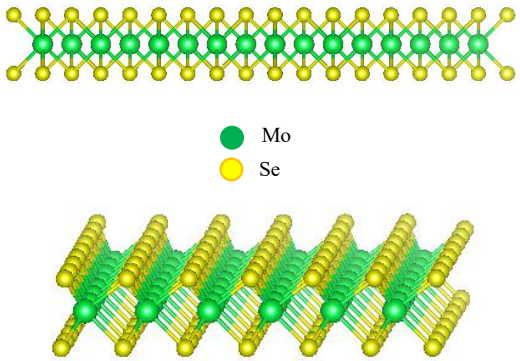

Fig. 1. Crystal structure of $MoSe_2$.

$$T = exp\left(-\frac{4\lambda\sqrt{2m^*}\sqrt{E_g^3}}{3q\hbar(E_g+\Delta\varphi)}\right)$$

where m^* is the effective mass of the charge carrier, λ is the screening length and $\Delta\phi$ is the tunneling window. The exponential dependence of the tunneling probability and tunneling current on E_g gives a unique opportunity to design ultrasensitive strain sensor using $MoSe_2$ TFET. To this end, it is important to first evaluate the impact of strain on electrical characteristics of $MoSe_2$ based TFETs. The impact of the strain on the transfer characteristics of WSe_2 TFET has been briefly presented in past, without much explanation about the physics behind the strain dependence of the device performance [25]. Herein, we demonstrate that the uniaxial strain impacts the band gap as well as the effective mass of the charge carrier, resulting in the strain dependent performance of $MoSe_2$ TFET. Further, we demonstrate that this strain dependence property of $MoSe_2$ TFET can be utilized to design a highly sensitive strain sensor and to improve the circuit level performance like delay and energy-delay product of the device.

This paper is arranged as follows: Section II studies the impact of uniaxial strain on the material parameters of $MoSe_2$ using the first principle density functional theory (DFT) calculation under meta generalized gradient approximation (MGGA) using the QuantumATK simulation tool [26]. Specifically, a hexagonal unit cell of $MoSe_2$ is considered for the DFT simulation with a *k*-point sampling of Brillouin zone along the path Γ→M→K→Γ→A→L→H→A and 20 sampling point in each path (*e.g.* 20 sample point in Γ→M path, 20 sample point in M→K path, etc., total 140 *k*-point). The vacuum layer is kept fixed at 10 A^0. The criteria for convergence of atomic forces have been considered to be 1×10^{-6} Ry. The comparison of calculated electronic parameters with the literature data is presented in Table I. Then the device

Table I. Comparison of the DFT calculated electronic parameters with the literature data

Electronic parameters	Calculated value (This work)	Ref. [30]
Band gap	1.39	1.48
Effective mass of electron	0.58	0.56
Effective mass of hole	0.72	0.66

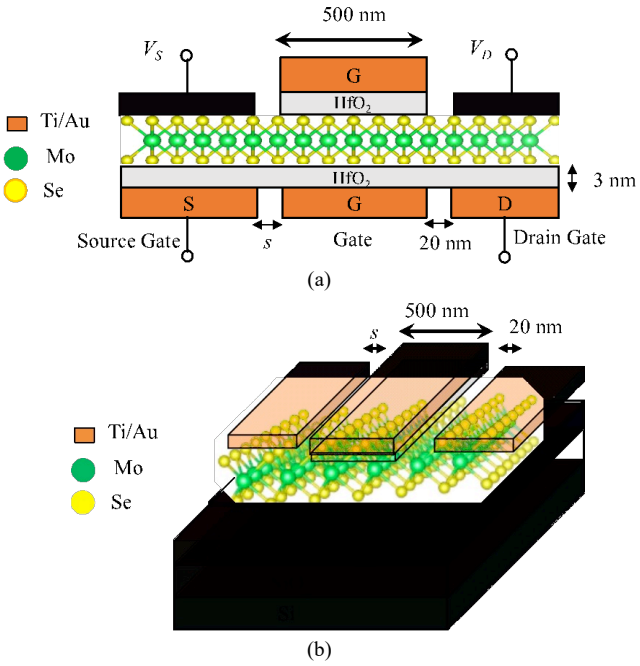

Fig. 2. (a) A 2-D schematic of $MoSe_2$ based TFET structure (b) 3-D structure of $MoSe_2$ TFET, the top and bottom gate oxide thickness is kept fixed at 3 nm..

performance at different mechanical strain conditions is studied Section III. The electrical parameters like transfer characteristics, subthreshold swing (*SS*) versus I_{DS} characteristics, and sensitivity of the device to the strain have been investigated. The results demonstrate that by applying a uniaxial tensile strain, the I_{ON} of TFET increases the speed and the energy efficiency of the device. The device shows a sensitivity ($\Delta I_{DS}/I_{DS}$) of 3.61 for a strain of 2% that is maximum when compared with other state-of-art devices like reduced graphene oxide (rGO) FET and organic FET based strain sensors [27], [28].

II. Material Modeling and Simulation Approach

The device structure of $MoSe_2$ based TFET is presented in Fig. 2. The voltages of 2 V and -1V are applied to the source- and drain-gate terminals to allow doping of $MoSe_2$ under source and drain regions. The performance of $MoSe_2$ based TFET has been investigated by solving the 3D Poisson and Schrodinger equation in NEGF framework with the tight binding (TB) Hamiltonian. Two band Hamiltonian parameters of the $MoSe_2$ has been calculated using electron effective mass (m_e), hole effective mass (m_h) and energy band gap (E_g). The value of m_e, m_h and E_G of $MoSe_2$ in relax condition is considered as 0.58 m_0, 0.72 m_0, and 1.39 eV, respectively. All device simulations were performed using an open source simulation tool NanoTCAD ViDES [29]. The two band Hamiltonian of $MoSe_2$ can be defined as:

$$H_{MoSe_2} = \begin{bmatrix} E_C + \frac{\hbar^2 k^2}{2m_0} & tf(k) \\ tf^*(k) & E_V + \frac{\hbar^2 k^2}{2m_0} \end{bmatrix}$$

where E_C and E_V are the bottom of the conduction band and top of the valance band, respectively. The in-plane hoping energy

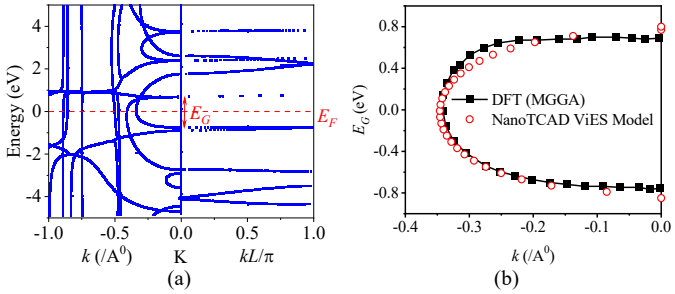

Fig. 3 (a) Complex band diagram of MoSe2 (b) Comparison of NanoTCAD ViDES model with the most relevant branch of the imaginary dispersion.

is represented by t, which depends on the effective mass and the bandgap of $MOSe_2$ and $f(k)$ is function due to nearest neighbor. For non-trivial solution of the crystal states of WTe_2, the following conditions must be satisfied:

$$\left|H - E(k)I\right| = 0$$

$$\begin{vmatrix} E_C + \dfrac{\hbar^2 k^2}{2m_0} - E(k) & tf(k) \\ tf^*(k) & E_V + \dfrac{\hbar^2 k^2}{2m_0} - E(k) \end{vmatrix} = 0 \qquad (1)$$

since in semiconductors, m_0 is much larger than the effective mass of the electron that results in much smaller $\hbar^2 k^2 / 2m_0$ in comparison to $\hbar^2 k^2 / 2m^*$. Therefore, it is assumed that $\hbar^2 k^2 / 2m_0$ is negligible in comparison to $E(k)$ and the Hamiltonian of $MoSe_2$ reduces to the form:

$$H_{MoSe_2} = \begin{bmatrix} E_C & tf(k) \\ tf^*(k) & E_V \end{bmatrix} \qquad (2)$$

where E_C and E_V are the bottom of the conduction and valence band edges, t is the in-plane hoping energy, and $f(k)$ is a function that represents the effect of nearest neighbor. The function $f(k)$ can be expressed as:

$$f(k) = e^{(ik_y a/\sqrt{3})} + 2e^{(-ik_y a/2\sqrt{3})} \cos\left(\frac{k_x a}{2}\right) \qquad (3)$$

where k_x and k_y are the wave vector along the x- and y-directions, a is the distance between Mo and Se atoms. Using the secular equation, the two-band dispersion relation can be expressed as:

$$E^{\pm}(k) = \frac{(E_C + E_V) \pm \sqrt{(E_C - E_V)^2 + 4t^2 \left|f(k)\right|^2}}{2} \qquad (4)$$

The parabolic effective mass approximation is considered with the two-band model for calculation of Hamiltonian as:

$$\frac{1}{m_R} = \frac{1}{\hbar^2} \frac{\partial^2 E^{\pm}(k)}{\partial k_x^2} \qquad (5)$$

where m_R is the reduced mass of the electron and hole. Using Eqs. (2)-(4), and assuming the limit of second derivatives at the minimum energy k-points, the value of t can be expressed as:

$$\left|t\right|^2 = \frac{2\hbar^2 E_g}{3a^2 m_R} \qquad (6)$$

where m_R is the reduced effective mass of electron and hole and can be expressed by the expression:

$$\frac{1}{m_R} = \frac{1}{m_e} + \frac{1}{m_h}$$

Solving Eq. (2), (4), and (5), we obtain the wave vector as

$$k_x = \frac{2}{a}\cos^{-1}\left(-\frac{1}{2}\cos\frac{\sqrt{3}k_y a}{2} + \sqrt{\frac{1}{4}\left(\cos^2\frac{\sqrt{3}k_y a}{2} - 1\right) + \frac{3a^2 m_R^*}{8\hbar^2 E_g}\left(E_V - E(k)\right)\left(E_C - E(k)\right)}\right) \qquad (7)$$

The imaginary wave vector in the material can be expressed as:

$$\mathrm{Im}(k_x) = \frac{2}{a}\cosh^{-1}\left(\frac{1}{\cos\dfrac{a\,\mathrm{Re}(k_x)}{2}}\sqrt{\frac{1}{4}\left(\cos^2\frac{\sqrt{3}k_y a}{2} - 1\right) + \frac{3a^2 m_R^*}{8\hbar^2 E_g}\left(E_V - E(k)\right)\left(E_C - E(k)\right)}\right) \qquad (8)$$

To validate the model for $MoSe_2$, we have compared the imaginary E-k curve obtained using (6) with the most relevant branch of the complex band structure (Fig. 3) obtained from DFT simulation under TB09 meta-GGA (MGGA) approximation. It is observed that the NanoTCAD ViDES result is consistent with the first principle DFT calculation result.

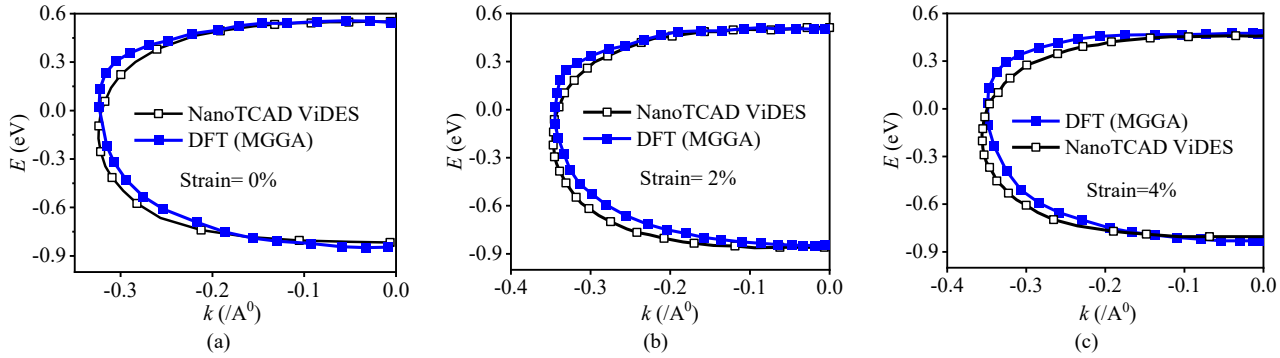

Fig. 4. Imaginary branch of E-k diagram in (a) relax condition (b) in 2% strain (c) at 4% strain condition

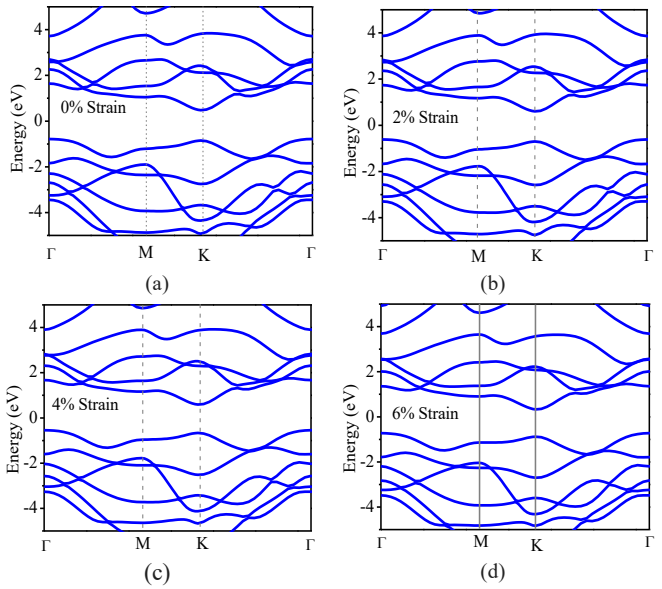

Fig. 5. Band diagram of $MoSe_2$ at strain of (a) 0% (b) 2% (c) 4% (d) 6%.

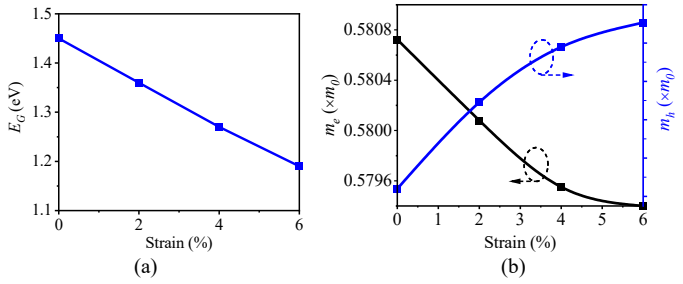

Fig. 6. Impact of strain on (a) band gap (b) electron and hole effective masses

Further, the comparison of *E-k* curve obtained using tight binding model (7) in strained conditions and DFT calculation is presented in Fig. 4. It can be observed that the NanoTCAD results are in good agreement with the DFT results in strain conditions also. This shows that the tight-binding model is capable to capture the strain effects in the electronic structure of $MoSe_2$.

III. Results and Discussion

The impact of the uniaxial strain on the band gap and effective masses of the semiconductor has been calculated using the first principle DFT method under MGGA approximation. The *E-k* dispersion relation of the $MoSe_2$ under the relaxed condition, and 2%, 4%, and 6% uniaxial tensile strain conditions are presented in Fig. 5. The *E-k* dispersion curves and their curvatures are used to calculate the band gap and effective mass of the charge carriers. The variation in energy band gap of $MoSe_2$ with a percentage change in uniaxial strain is presented in Fig. 6 (a). It can be observed that the band gap decreases linearly with an increase in the uniaxial strain. The variation of the electron and hole effective masses with strain variation is presented in Fig. 6 (b). The effective mass of electron shows a very small variation of $0.5807m_0$ to $0.5794m_0$ with a change in the strain from 0% to 5%, while the uniaxial strain has a dominating impact on the effective mass of hole and it changes from $0.720m_0$ to $1.153m_0$. However, such variations do not

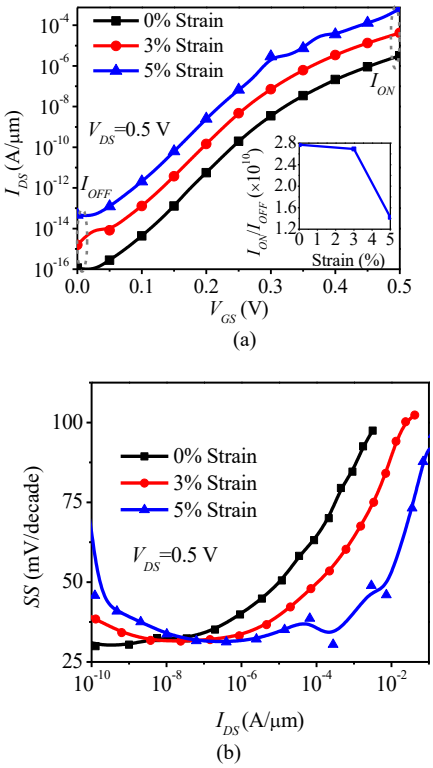

Fig.7. Impact of strain on (a) the transfer characteristics and (b) *SS* versus I_{DS} characteristics of the MoSe2 based TFET at V_{DS}=0.5 V at a fixed *s* of 4 nm.

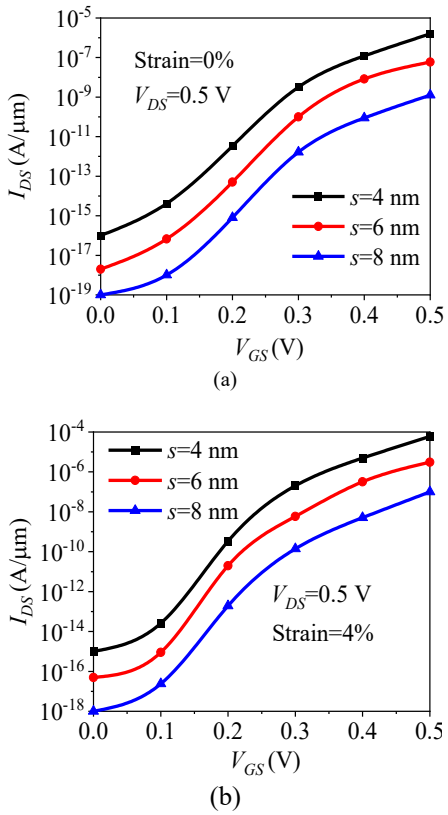

Fig. 8. Impact of source-drain metal gap (*s*) on transfer characteristics in (a) zero strain and (b) 4% strain conditions

affect the performance of the device significantly since the tunneling current is dominated by electrons. As the curvature of the valence band at Γ point is smaller than the curvature of the conduction band at the K-point, the effective mass of the hole remains higher than the effective mass of the electron in all

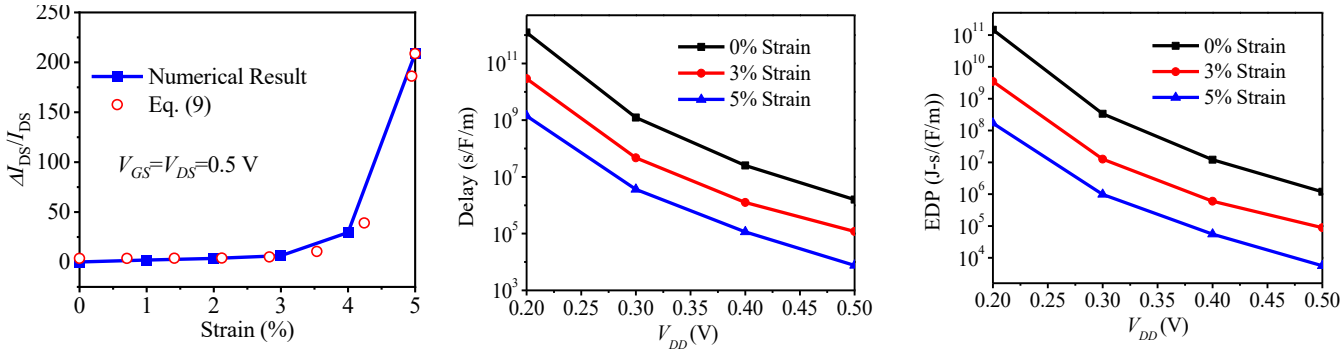

(a) (b) (b)

Fig.9. Impact of strain on the (a) sensitivity ($\Delta I_{DS}/I_{DS}$) of the MoSe2 TFET of 10 stage inverter chain (b) delay and (c) energy-delay product of 10 stage inverter chain

strain conditions. The calculated band gap and effective masses have been used to study the device performance of TFET at different strain conditions. The impact of strain on transfer and *SS* versus I_{DS} characteristics are presented in Fig. 7. It can be noted that the I_{ON} and I_{OFF} increases with the increase of external strain while the I_{ON}/I_{OFF} ratio remains nearly the same (inset Fig. 7a). Such increase in the drain current with mechanical strain is attributed to the decrease in energy band gap of $MoSe_2$ as discussed previously in Fig. 5. On the other hand, the *SS* of $MoSe_2$ TFET at higher strain conditions remains low for a wide range of drain current. Under all the strain conditions, the SS of the device can be as low as ~25 mV/dec, which is comparable to the best reported results so far [18]-[19], [21]-[22]. The impact of source-gate metal gap (*s*) on the performance of the device in strained and zero strain conditions is presented in Fig. 8. It can be observed that the *s* is a crucial parameter in electrostatic doping based TFET design and need to be controlled to avoid the variability issues. The sensitivity of the device ($\Delta I_{DS}/I_{DS}$) as a function of mechanical strain is presented in Fig. 9 (a). The $MoSe_2$ TFET shows a high sensitivity to the applied strain. The nonlinear variation in sensitivity of $MoSe_2$ TFET is due to the exponential dependence of TFET current on the energy band gap. By empirical curve fitting of the sensitivity versus strain curve, it is observed that the sensitivity exponentially depends on the strain (ϵ) as:

$$\frac{\Delta I_{DS}}{I_{DS}} = A_1 + A_2 \exp\left(-\epsilon/B\right) \tag{9}$$

where A_1, A_2 and B are constants and have values of 3.60, 0.0019 and -0.43 respectively. The Eq. (9) can also be used to determine the sensitivity of the device. A comparison of the key performance parameters of the $MoSe_2$ TFET sensor with the reported strain sensors are presented in Table II. It can be observed that the $MoSe_2$ TFET shows maximum sensitivity in comparison to organic FET and graphene FET to the mechanical strain and operates at a comparatively lower supply voltage. In fact, the strain sensitivity of 9 times higher than the value reported for Pentacene based organic FET. These results indicate that the external strain could be used as stimuli to modulate the channel current and in this regard the presented FET could also be used as a strain sensor. The modulation of device channel current by external stimuli such as touch/contact force, temperature and even chemicals has been used in past to obtain highly sensitive physical and chemical sensors [4], [31]-[35]. Further, we have studied the impact of the strain on the performance of the TFET based 10 stage inverter chain (Fig. 9b and Fig. 9 c) assuming symmetric *n*TFET and *p*TFET structures [21]. The normalized delay and energy per operation can be written as [36], [37].

Table II. Comparison of performance parameters with reported strain sensors.

Performance Indicators	**Reduced Graphene oxide FET [27]**	**Pentacene based Organic FET [28]**	**P3HT based Organic FET [28]**	**MoSe2 TFET (This work)**
Strain	0.35%	2%	2%	2%
Sensitivity ($\Delta I_{DS}/I_{DS}$)	0.03	0.4685	0.08536	3.61
Operating Voltage	3 V	10 V	10 V	0.5 V

$$E = V_{DD}^2\left(\alpha + L_D\frac{I_{OFF}}{I_{ON}}\right) \tag{10}$$

where $t_p = V_{DD}L_D/I_{ON}$ is the normalized delay of the the inverter chain, L_D is the number of stages, E is the normalized energy per operation, α is the activity factor, and V_{DD} is the supply voltage. We have compared the delay versus V_{DD} and energy-delay product (EDP) versus V_{DD} characteristics of TFET in 0%, 3% and 5% strain conditions. The α was fixed at 3% for a fair comparison. The speed and energy-delay product (EDP) of the circuit decreases with increase in the uniaxial mechanical strain. This improvement in delay and EDP of the inverter chain is attributed to the decrease in band gap with an increase in uniaxial mechanical strain that enhance the ON current of the device. Therefore, the circuit performance of $MoSe_2$ TFET can be potentially improved by applying a controlled mechanical strain on the device using an external force. As a single device, the proposed $MoSe_2$ TFET can be used as a strain sensor, but when put together in the circuit under controlled strain conditions they lead to high-performance and low power applications. In contrast to conventional FET technology where carrier transport is due to thermionic injection, the TFETs shows weaker dependence on the temperature variations due to band-to-band tunneling based carrier injection mechanism [38]. Therefore, the response of device is tolerant to temperature variations when used in the circuits.

IV. Conclusion

This paper investigates the impact of mechanical strain on the

$MoSe_2$ based TFET structure. The device displayed a steep slope with SS down to ~ 30 mV/dec. This is significantly lower than the Boltzmann limit (60 mV/decade) at room temperature and comparable to the best reported TMD based FET. With external uniaxial strain, the I_{ON} and I_{OFF} of $MoSe_2$ TFET increased with the increase in strain while the steep slope (thus SS) remains robust. With these results, the presented device shows a potential for strain sensing application with an exponential dependence between the sensitivity of the device and the applied strain. Further, the enhancement of I_{ON} under strain condition can be utilized to reduce delay and energy-delay product of TFET based circuits. A case study of strained TFET based 10-stage inverter chain clearly demonstrates an improvement of the speed and energy efficiency.

REFERENCES

[1] R. Dahiya, L. Manjakkal, F. Liu, N. Yogeswaran, E. Burdet, V. Hayward, H. Jorntell, "Large area soft eskin: The challenges beyond sensor designs," *Proceedings of the IEEE*, vol. 107, no. 10, pp. 2016-2033, 2019.

[2] Chen Jiang, Hyung Woo Choi1, Xiang Cheng, Hanbin Ma, David Hasko1, Arokia Nathan, "Printed subthreshold organic transistors operating at high gain and ultralow power," *Science*, vol. 363, no. 6428, pp. 719-723, 2019.

[3] H.-P. Phan, Y. Zhong, T.-K. Nguyen, Y. Park, T. Dinh, E. Song, R.K. Vadivelu, M.K. Masud, J. Li, M.J.A. Shiddiky, D. Dao, Y. Yamauchi, J.A. Rogers and N.-T. Nguye, "Long-lived, transferred crystalline silicon carbide nanomembranes for implantable flexible electronics," *ACS Nano* vol. 13, pp. 11572-11581, 2019.

[4] N. Yogeswaran, W. T. Navaraj, S. Gupta, F. Liu, V. Vinciguerra, L. Lorenzelli, and R. Dahiya, "Piezoelectric graphene field effect transistor pressure sensors for tactile sensing," *Appl. Phys. Lett.*, vol. 113, no. 1, p. 014102, 2018.

[5] F. Liu, W. T. Navaraj, N. Yogeswaran, D. H. Gregory, and R. Dahiya, "van der Waals contact engineering of graphene field-effect transistors for large-area flexible electronics," *ACS Nano*, vol. 13, no. 3, pp. 3257–3268, 2019.

[6] W. T. Navaraj, S. Gupta, L. Lorenzelli, and R. Dahiya, "Wafer scale transfer of ultrathin silicon chips on flexible substrates for high performance bendable systems," *Adv. Electron. Mater.*, vol. 4, no. 4, p. 1700277, 2018.

[7] C. García Núñez, F. Liu, W. T. Navaraj, A. Christou, D. Shakthivel, and R. Dahiya, "Heterogeneous integration of contact-printed semiconductor nanowires for high-performance devices on large areas," *Microsystems Nanoeng.*, vol. 4, no. 22, pp. 1-15, 2018.

[8] S. Khan, L. Lorenzelli, R. Dahiya, "Technologies for Printing Sensors and Electronics Over Large Flexible Substrates: A Review," *IEEE Sensors J.*, vol. 15, no. 6, pp 3164-3185, 2015.

[9] S. Gupta, W. T. Navaraj, L. Lorenzelli, R. Dahiya, "Ultra-thin chips for high-performance flexible electronics," *NPJ Flexible Electronics*, vol. 2, no. 8, pp. 1-17, 2018.

[10] W. Cao, J. Jiang, X. Xie, A. Pal, J. H. Chu, J. Kang, K. Banerjee, "2-D layered materials for next-generation electronics: Opportunities and challenges," *IEEE Trans. Electron Devices*, vol. 65, no. 10, pp. 4109–4121, 2018.

[11] F. W. Chen, H. Ilatikhameneh, G. Klimeck, Z. Chen, and R. Rahman, "Configurable electrostatically doped high performance bilayer graphene tunnel FET," *IEEE J. Electron Devices Soc.*, vol. 4, no. 3, pp. 124–128, 2016.

[12] H. Ilatikhameneh, G. Klimeck, J. Appenzeller, and R. Rahman, "Scaling theory of electrically doped 2D transistors," *IEEE Electron Device Lett.*, vol. 36, no. 7, pp. 726–728, 2015.

[13] E. O. Polat, O. Balci, N. Kakenov, H. Burkay Uzlu, C. Kocabas, R. Dahiya, "Synthesis of large area graphene for high performance in flexible optoelectronic devices," *Scientific Reports*, vol 5, no. 16744, pp. 1-10, 2015.

[14] H. Xu, X. Han, W. Liu, P. Liu, H. Fang, X. Li, Z. Li, J. Guo, B. Xiang, W. Hu, I. P. Parkin, J. Wu, Z. Guo, H. Liu, "Ambipolar and Robust WSe2 Field-Effect Transistors Utilizing Self-Assembled Edge Oxides" *Advan. Mat. Interfaces,* vol. 7, no. 1, pp. 1901628, 2020.

[15] K.-A. N. Duerloo , Y. Li and E. J. Reed, "Structural phase transitions in two-dimensional Mo- and W-dichalcogenide monolayers," Nature Communications, vol. 5, no. 4214, pp. 1-9, 2014.

[16] Y. Zhang, T.-R. Chang, B. Zhou, Y.-T. Cui, H. Yan, Z. Liu, F. Schmitt, J. Lee, R. Moore, Y. Chen, H. Lin, H.-T. Jeng, S.-K. Mo, Z. Hussain, A. Bansil and Z.-X. Shen , "Direct observation of the transition from indirect to direct bandgap in atomically thin epitaxial $MoSe_2$," *Nature Nanotech.,* vol. 9**,** pp. 111–115, 2014.

[17] P. Johari and V. B. Shenoy, "Tuning the electronic properties of semiconducting transition metal dichalcogenides by applying mechanical strains," *ACS Nano*, vol. 6, no. 6, pp. 5449–5456, 2012.

[18] A. Vilouras, H. Heidari, S. Gupta, R. Dahiya, "Modelling of CMOS devices and circuits on flexible ultra-thin chips," *IEEE Trans. Electron Devices*, vol. 65, no. 5, pp. 2038-2046, 2017.

[19] H. Heidari, N. Wacker, R. Dahiya, "Bending induced variations in ultra-thin flexible chips and device modeling," *Applied Physics Rev*., vol 4, no. 031101, 2017.

[20] S. Deng, L. Li, M. Li "Stability of direct band gap under mechanical strains for monolayer MoS2, MoSe2, WS2 and WSe2," *Physica E: Low-dimensional Systems and Nanostructures*, vo. 101, pp. 44-49, 2018.

[21] A. M. Ionescu and H. Riel, "Tunnel field-effect transistors as energy-efficient electronic switches," *Nature*. pp. 329–337, 2011.

[22] P. K. Dubey and B. K. Kaushik, "T-shaped III-V heterojunction tunneling field-effect transistor," *IEEE Trans. Electron Devices*, vol. 64, no. 8, pp. 3120–3125, 2017.

[23] P. K. Dubey and B. K. Kaushik, "A charge plasma-based monolayer transition metal dichalcogenide tunnel FET," *IEEE Trans. Electron Devices*, vol. 66, no. 6, pp. 2837–2843, 2019.

[24] D. Sarkar *et al.*, "A subthermionic tunnel field-effect transistor with an atomically thin channel," *Nature*, vol. 526, no. 7571, pp. 91–95, 2015.

[25] H. Ilatikhameneh, G. Klimeck, J. Appenzeller, and R. Rahman, "Design rules for high performance tunnel transistors from 2-D materials," *J. Electron Devices Soc*., vol. 4, no. 6, pp. 260–265, 2016.

[26] *Quantum Wise Simulator*, Atomistic Tool Kit (ATK). [Online]. Available: http://www.quantumwise.com/

[27] T. Q. Trung, N. T. Tien, D. Kim, M. Jang, O. J. Yoon, and N. Lee, "A flexible reduced graphene oxide field-effect transistor for ultrasensitive strain sensing," *Advnced Funct. Mater.*, vol. 24, pp. 117–124, 2014.

[28] P. Cosseddu, S. Milita, and A. Bonfiglio, "Strain sensitivity and transport properties in organic field-effect transistors," *IEEE Electron Device Lett.*, vol. 33, no. 1, pp. 113–115, 2012.

[29] "NanoTCAD ViDES." [Online]. Available: http://vides.nanotcad.com/vides. [Accessed: 20-Jul-2017].

[30] X.-W. Jiang, J.-W. Luo, S.-S. Li, and L.-W. Wang, "How good is monolayer transition-metal dichalcogenide tunnel field-effect transistors in sub-10 nm?—An ab initio simulation study," in *IEDM Tech. Dig.*, Dec. 2015, pp. 12.4.1–12.4.4.

[31] Gupta, N. Yogeswaran, F. Giacomozzi, L. Lorenzelli, R. Dahiya, "Touch sensor based on flexible AlN piezocapacitor coupled with MOSFET," *IEEE Sensors J*., 2019, DOI: 10.1109/JSEN.2019.2928797

[32] S. Gupta, D. Sakthivel, L. Lorenzelli, R. Dahiya, "Temperature compensated tactile sensing using MOSFET with P(VDF-TrFE)/BaTiO3 capacitor as extended gate," *IEEE Sensors J*., vol. 19, no.2, pp. 435-442, 2018.

[33] S. Gupta, D. Sakthivel, L. Lorenzelli, R. Dahiya, "Temperature compensated tactile sensing using MOSFET with P(VDF-TrFE)/BaTiO3 capacitor as extended gate," *IEEE Sensors J*., vol. 19, no. 2, pp. 435-442, 2018.

[34] S. Hannah, D. Uttamchandani, R. Dahiya, H. Gleskova "Multifunctional sensor based on organic field-effect transistor and ferroelectric poly(vinylidene fluoride trifluoroethylene) Organic Electronics," *Organic Electronics*., vol. 56, pp 170-177, 2018.

[35] Nicolas Moser, Tor Sverre Lande, Christofer Toumazou, Pantelis Georgiou," ISFETs in CMOS and emergent trends in instrumentation: A review ," *IEEE Sensors J*., vol. 16, no. 17, 2016.

[36] T. Agarwal, I. Radu, P. Raghavan, G. Fiori, A. Thean, M. Heyns, and W. Dehaene, "Effect of material parameters on two-dimensional materials based TFETs: An energy-delay perspective," in *Proc. Eur. Solid-State Device Res. Conf. (ESSDERC)*, 2016, pp. 47–50.

[37] T. K. Agarwal, B. Soree, I. Radu, P. Raghavan, G. Iannaccone, G. Fiori, W. Dehaene, and M. Heyns, "Material-device-circuit co-optimization of 2D material based FETs for ultra-scaled technology nodes," *Sci. Rep*., vol. 7, no. 5016, Jul. 2017,.

[38] P. Wu, T. Ameen, H. Zhang, L. A. Bendersky, H. Ilatikhameneh, G Klimeck, R. Rahman, A. V. Davydov, and J. Appenzeller,

"Complementary black phosphorus tunneling field-effect transistors," *ACS Nano*, vo. 13, pp. 377−385, 2019.